FUNCTIONALIZED SUB-10 NM SILICA METHYLENE BLUE NANOPHOTOSENSITIZERS

A Thesis

Presented to the Faculty of the Graduate School

of Cornell University

In Partial Fulfillment of the Requirements for the Degree of

Master of Science

by

Songying Li

August 2018

ABSTRACT

Photodynamic therapy (PDT) presents an alternative non-invasive therapeutic modality for the treatment of cancer and other diseases. PDT relies on cytotoxic singlet oxygen that is locally generated through energy transfer between a photosensitizer and molecularly dissolved triplet oxygen. To minimize side-effects, *i.e.* damage of healthy tissue, targeted delivery to places of disease, high local photosensitizer concentrations, high singlet oxygen quantum yield, and rapid post-treatment clearance of photosensitizers are desired. Ultrasmall (sub-10 nm) organic-inorganic hybrid silica nanoparticles loaded with photosensitizer molecules, referred to as silica nanophotosensitizers (SNPSs), present a way to meet these requirements. Here, we investigate two different particle designs of ultrasmall poly(ethylene glycol) coated (PEGylated) SNPSs covalently binding the methylene blue derivate MB2. In the first approach (design one), MB2 is encapsulated into the silica matrix, while in the second approach (design two), MB2 is grafted on the particle surface in between chains of the stabilizing PEG corona. We compare both cases with regard to their singlet oxygen quantum yields, Φ_{Δ}, with the effective Φ_{Δ}^{eff} per particle reaching 111% and 161% for design one and two, respectively. Finally, we show that both particle designs allow functionalization with a targeting peptide, c(RGDyC), rendering SNPSs a promising platform for medical applications.

BIOGRAPHICAL SKETCH

Songying Li is from Shanghai, China. He earned his Bachelor of Science degree in materials science and engineering at Shanghai Jiao Tong University in China before enrolled in Master of Science program at Cornell.

During his undergraduate program, his research mainly focused on polymer nanoparticles self-assembly in cancer treatment. In this period, he learned many experimental skills relative to polymer and nanoparticle synthesis and characterization including DLS, UV-vis, NMR and TEM. The results of his research were included in a published paper *Self-Assembly Assisted Fabrication of Dextran-Based Nanohydrogels with Reduction- Cleavable Junctions for Applications as Efficient Drug Delivery Systems* in Scientific Research in 2017.

Pursuing his master's degree at Cornell, he entered Professor Wiesner's group to study ultra-small fluorescent silica nanoparticles, well known as "Cornell dots" or simply C'dots. His project aimed to functionalize C' dots as a platform to perform photodynamic therapy for cancer by incorporating photosensitizer dyes in the silica matrix and enabling C' dots as a highly biocompatible targeting carrier. After completing his master program with two submitted manuscripts, he plans to enroll in the PhD program in materials science and engineering at the University of Wisconsin, Madison.

ACKNOWLEDGMENTS

The completion of my master program won't occur without the strong support of my academic committee Professor Ulrich Wiesner, Chairperson and Professor Lara Estroff, Minor Advisor. At the same time, I want to express my appreciation to all Wiesner Group colleagues as well as friends, especially Dr. Ferdinand Kohle and Joshua Hinckley for mentoring my experiments and research. This work also made use of the Cornell Center for Materials Research (CCMR) shared facilities at Cornell. What's more, I would like to thank all administrative faculties for their timely assistance during my school life at Cornell. Finally, I want to express huge gratitude to my family who support me financially and mentally all the time and my friends with whom I shared an unparalleled two-year life in Ithaca.

TABLE OF CONTENTS

CHAPTER 1

OVERVIEW

1.1 History and Development of PDT

Photodynamic therapy (PDT) refers to a combination of light and a photosensitive reagent called photosensitizer (PS) to treat diseases [1]. People have utilized the therapeutic properties of light for three thousand years to treat different diseases including psoriasis, rickets, vitiligo and skin cancer in ancient Egypt, India and China [2]. Modern light therapy was introduced by Niels Finsen at the end of the nineteenth century, who found that the formation and discharge of smallpox pustules could be prevented by being exposed to red light, leading to a Nobel Prize award in 1903. In the next hundred years, scientists and researchers developed those light induced methods into a combination of light and certain chemicals to cause cell death after the introduction of the term 'photodynamic' by Von Tappeiner and A. Jesionek (Figure 1).

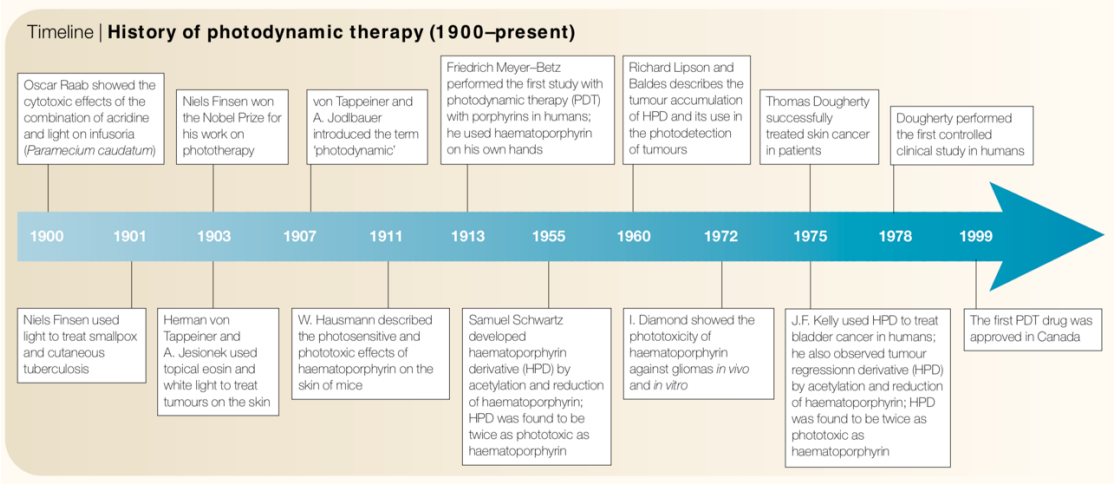

Figure 1. A simplified timeline for the history of photodynamic therapy [1].

Modern PDT was initiated by Frederich Meyer-Berz in 1913 who first tested PDT in humans, followed by Richard Lipson in the 1960s who studied a photosensitive compound called hematoporphyrin derivative (HPD) that could be selectively localized and accumulated in tumor sites [3][4][5]. However, it was not until the 1970s that scientists and researchers figured out the therapeutic application of PDT to patients with cancer [6]. After that, with a large amount of hard work from scientists all over the world, the efficiency of PDT has been gradually improved by developing more selective and potent photosensitizers and advanced research equipment.

PDT consists of two individually non-toxic components: photosensitizer (PS) and light. Absorption of light at certain wavelength excites PS molecules from the ground state to a triplet excited state. Through collisions in the excited state PS molecules transfer energy to ground state oxygen thereby generating reactive oxygen species (ROS), such as singlet oxygen and free radicals. Those ROS show cellular toxicity and lead to apoptosis or cell death. PSs can be divided into two types by the mechanism of singlet oxygen generation [7]. Type I mechanism involves an intermediate macromolecule which reacts with a PS first as a carrier of excited electrons or hydrogen atoms and then transfers them to molecular triplet oxygen to form cytotoxic reactive oxygen species (ROS). On the other hand, type II mechanism involves direct energy transfer reaction between a PS and molecular ground state oxygen. PDT induces tumor damage through three main pathways: (i) the ROS generated by PDT directly kill tumor cells; (ii) PDT damages the tumor-associated vasculature, leading to tumor infarction; (iii) PDT activates an immune response against tumor cells.

1.2 Thesis Overview

In this thesis, a well-established nanoparticle platform, i.e. Cornell prime dots (C' dots), was utilized as a new carrier of PSs to localize and accumulate them in specific tumor sites (for their synthesis see Figure 2). Well known as ultrasmall sub-10nm PEGylated fluorescent core-shell silica nanoparticles that have been translated into the clinic, sophisticated particle size control in the sub-10 nm region has successfully been reported as well as a versatile surface modification approach to modularly and orthogonally functionalize C' dots with up to four types of different functional ligands on the particle surface [8]. Designed as nanoparticles integrating a variety of properties including fluorescence detection, specific cell targeting, radioisotope chelating/labeling, ratiometric pH sensing, and drug delivery [8], C' dots are chosen to be a novel PS carrier by either incorporating PS molecules inside the silica core or grafting PS molecules on the surface among the PEG corona.

Here, we introduce ultrasmall sub-10 nm organic-inorganic hybrid SNPs covalently binding the PS dye MB2, a derivate of methylene blue (MB) (Figure 3B and Figure A1). In the following we will refer to these particles as silica nanophotosensitizers (SNPSs). MB is a PS molecule that is FDA-approved and has been used in photodynamic therapy [9][10], due to its high singlet oxygen quantum yield and extinction coefficient in the near infrared ($\Phi_\Delta \approx 0.5$, $\varepsilon = 10^5\ M^{-1}\ cm^{-1}$ at 664 nm). Despite earlier attempts to synthesize MB containing SNPs, to the best of our knowledge sub-10 nm functionalized SNPs covalently binding MB have not been reported to date [11][12][13].

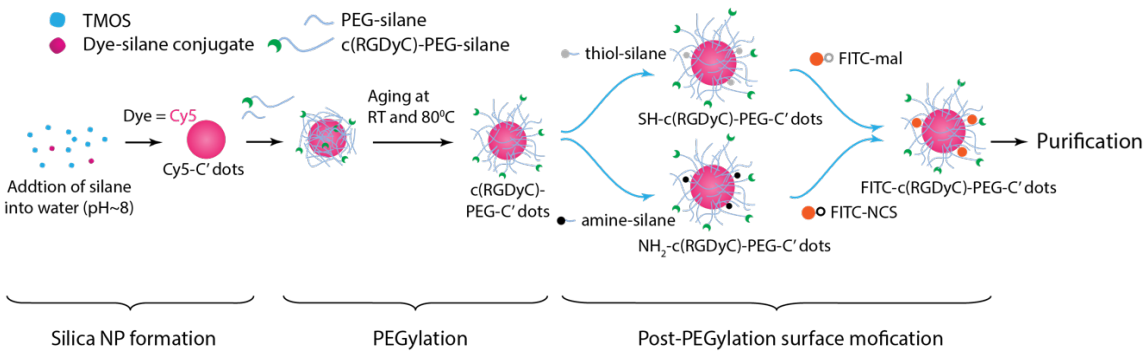

Figure 2. Illustration of C' dot synthesis system with Cy5 and FITC as examples of primary and secondary dyes.

We demonstrate two different SNPS designs (Figure 3C). In design one, MB2 is encapsulated within the silica network of an ultrasmall poly(ethylene glycol) coated (PEGylated) SNP; in design two, MB2 is grafted onto the SNP surface, inserted between the PEG corona chains. In both cases the PS molecules are covalently bound to the SNPSs via a thiol-Michael addition click reaction between maleimide functionalized MB2 and (3-mercaptopropyl)trimethoxysilane (MPTMS). We show that both particle types can be further functionalized with the $\alpha_v\beta_3$ integrin-targeting cyclic(arginine-glycine-aspartic acid-D-tyrosine-cysteine) peptide (cRGDyC, Figure 3D). Photosensitizing action is successfully demonstrated using the singlet oxygen sensor 1,3-diphenylisobenzofuran (DPBF, inset Figure 5A). We demonstrate effective per particle singlet oxygen quantum yields of 111% (design one) and 161% (design two), respectively.

CHAPTER 2

INTRODUCTION

2.1 Background

Photodynamic therapy (PDT) emerged as a minimally invasive and minimally toxic therapeutic modality for the treatment of cancer and other diseases [1]. The principle of PDT can generally be described in four steps: A photosensitizer (PS) is localized around diseased tissue (step 1) and activated by a light source (step 2). The absorbed photon energy leads to the generation of highly reactive singlet oxygen, $^1O_2$ (step 3), causing oxidative stress and cellular damage, eventually initiating cell death mechanisms such as necrosis and/or apoptosis in the local environment of the PS (step 4) [14]. These steps impose chemical, photophysical, and structural requirements onto PDT probes.

Photophysical requirements: A PS has unique photophysical characteristics. Generation of $^1O_2$ is catalyzed by photoexcitation of the PS. Figure 3A depicts a simplified Jablonski scheme illustrating the photophysical processes leading to $^1O_2$ generation. From an electronically excited singlet state the PS undergoes a forbidden electron spin-flip (intersystem crossing, ISC) into an energetically lower lying excited triplet state, ^{3}PS*. From here, ^{3}PS* relaxes into the singlet ground state, ^{1}PS, via energy transfer (ET) with dissolved molecular triplet oxygen, $^3O_2$, yielding cytotoxic reactive singlet oxygen, $^1O_2$. High intersystem crossing rates (k_{ISC}) and long triplet state lifetimes ($\tau_T > 1$ μs) of the PS promote $^1O_2$ generation, which is reflected in high singlet oxygen quantum yields, Φ_Δ [15]. An ideal PS should have a molar extinction coefficient of $\varepsilon \geq$

50 000 M^{-1} cm^{-1} [15][16] in the therapeutic window of ~600–1200 nm [17] and a singlet oxygen quantum yield of $\Phi_\Delta \geq 0.5$ [16]. In addition, high photostability, as well as low phototoxicity in the dark are desired.

Chemical requirements: Besides the general requirement of a PDT probe to be non-toxic itself, a key challenge is its localization at a specific site of interest. Singlet oxygen is highly reactive, and locally produced by the PS. Typical diffusion lengths of singlet oxygen in tissue before it reacts are on the order of tens of nanometers [18]. Therefore, to minimize damage of healthy tissue, selective targeting is crucial. Since most PS molecules are hydrophobic and prone to aggregation in physiological environments, low selectivity towards diseased tissue and adverse pharmacokinetics have hindered their clinical translation [19][20][16]. Nanoparticles (NPs) as PS delivery vehicles can promote solubility, overcome aggregation issues to improve pharmacokinetics, and protect PSs from enzymatic degradation [21][22]. Furthermore, NP surface functionalization with targeting moieties reduces systemic side effects, increases the therapeutic concentration of PSs at the target site, and gives room for multi-modality platforms simultaneously enabling diagnosis, imaging, and treatment [22]. However, while NP-based PS systems help overcome shortages associates with the PS molecules, they themselves impose additional requirements.

Structural requirements: First, since PSs are bound to NPs and don't have to be released, it is essential that oxygen species can easily diffuse to and away from the PS molecule. Second, after NPs have targeted the site of interest and PDT has been performed (or if the NPs have failed to target the site of disease in the first place) it is essential that they are rapidly cleared from the body to reduce potential side effects

(principle of *target-or-clear* [23]). Both of these requirements favor small hydrodynamic diameters leading to rapid renal clearance via the kidneys with a cutoff for spherical NPs below 10 nm hydrodynamic diameter [24].

2.2 Motivations

Different NP-based systems, organic, inorganic, and organic-inorganic hybrid, have been described in the literature, including PEGylated liposomes, polymeric NPs, iron oxide NPs, or gold NPs [7][25][26][27]. While numerous NPs systems are able to load large amounts of PS molecules, few NP platforms combine the necessary ease of chemical functionalization with precise particle size control on the sub-10 nm length scale, to meet stringent requirements for successful clinical translation and synthesis scale-up [28][29][30]. While metal-organic framework NPs in principle offer these capabilities, targeted delivery and systematic *in vitro* and *in vivo* studies on NP activity and fate demonstrating favorable characteristics are still lacking [31].

Ultrasmall organic-inorganic hybrid silica nanoparticles (SNPs) meet these requirements today. It has been demonstrated in first published human clinical trials that fluorescent sub-10 nm PEGylated and functionalized SNPs efficiently target and clear from the human body [32][33]. In addition, the chemical inertness, optical transparency of silica, and cost-effective water-based synthesis paired with exceptional size and structural control on the sub-nanometer length scale, insusceptibility to swelling due to pH changes, and high silica matrix porosity render such particles ideal candidates for PDT [8][17][34][35][36].

CHAPTER 3

METHODS AND RESULTS

3.1 Background

As ultrasmall PEGylated silica nanoparticles (C' dots) provide a potential platform as a satisfactory carrier to deliver photosensitizers into tumor site to apply PDT, we are interested in investigating the photo-properties of C' dots encapsulating photosensitizer dyes. In order to use the well-established syntheses of C' dot to incorporate the photosensitizer dye, a water-soluble and photostable photosensitizer is required. Here, for the photosensitizer, we choose MB2, a water-soluble Type II photosensitizer derived from methylene blue (MB) which lies advantage in its high singlet oxygen quantum yield and extinction coefficient in the near infrared ($\Phi_\Delta \approx 0.5$, $\varepsilon = 10^5\ M^{-1}\ cm^{-1}$ at 664 nm). Since MB has been approved for clinical translation by the U.S. Food and Drug Administration (FDA) and has been used in photodynamic therapy[9][10], it leaves potential of clinical translation for MB2 encapsulated C' dots as a novel PDT probe.

In this chapter, we introduce ultrasmall sub-10nm organic-inorganic hybrid silica nanoparticles (SNPs) covalently binding the photosensitizer dye MB2 (Figure 3B and Figure A1). In the following we will refer to these particles as silica nanophotosensitizers (SNPSs). We demonstrate two different SNPS designs (Figure 3C). In design one, MB2 is encapsulated within the silica network of an ultrasmall poly(ethylene glycol) coated (PEGylated) SNP; in design two, MB2 is grafted onto the SNP surface, inserted between the PEG corona chains. In both cases the PS molecules

are covalently bound to the SNPSs via a thiol-Michael addition click reaction between maleimide functionalized MB2 and (3-mercaptopropyl)trimethoxysilane (MPTMS). We show that both particle types can be further functionalized with the $\alpha_v\beta_3$ integrin-targeting cyclic(arginine-glycine-aspartic acid-D-tyrosine-cysteine) peptide (cRGDyC, Figure 3D). Photosensitizing action is successfully demonstrated using the singlet oxygen sensor 1,3-diphenylisobenzofuran (DPBF, inset Figure 5A). We demonstrate effective per particle singlet oxygen quantum yields of 111% (design one) and 161% (design two), respectively. Despite earlier attempts to synthesize MB containing SNPs, to the best of our knowledge sub-10 nm functionalized SNPs covalently binding MB have not been reported to date [9][37][38].

3.2 Materials and Methods

3.2.1 Materials

Aluminum-tri-sec-butoxide (ASB), (3-aminopropyl)triethoxysilane (APTES), ammonium hydroxide (28 wt% in H_2O), ammonia solution (2.0 M in ethanol), dimethyl sulfoxide (DMSO), 1,3-diphenylisobenzofuran (DPBF, 97%), hydrochloric acid (HCl, 0.5018 N in H_2O), (3-iodopropyl)trimethoxysilane (IPTMS), methylene blue (MB), (3-mercaptopropyl) trimethoxysilane (MPTMS), 2-propanol (anhydrous 99.5%), and tetramethyl orthosilicate (TMOS) were purchased from Sigma Aldrich. (3-aminopropyl)trimethoxysilane (APTMS) and methoxy-terminated poly(ethylene glycol) (PEG-silane, molar mass of ~0.5 kg/mol) were purchased from Gelest. Heterobifunctional PEG (NHS-PEG-mal, molar mass of ~960 g/mol) was purchased from Quanta BioDesign. ATTO MB2-maleimide was purchased from ATTO-Tec.

Tetramethylrhodamine-5-maleimide (TMR) was purchased from AnaSpec. Ethanol (absolute anhydrous 99.5%) was purchased from Pharmco-Aaper. c(RGDyC) was purchased from Peptide International. Deionized (DI) water (18.2 MΩ·cm) was generated using a Millipore Milli-Q system. All chemicals were used as received.

3.2.2 Synthesis of Nanophotosensitizers (Design One)

First, 3.67×10^{-7} moles MB2 with a maleimide group are reacted with MPTMS in DMSO at a molar ratio of 1:25 (fluorophore:MPTMS) to generate a MB2-silane conjugate. To synthesize sub-10 nm PEGylated SNPs with MB2 inside the silica core, 2 mL of 0.02 M ammonia aqueous solution is first added into 8 mL of DI water yielding a pH of ~9. The solution is then stirred at room temperature for 5 min. As the silica precursor, 0.43 mmol of TMOS are added under vigorous stirring, followed by the addition of all MB2-silane. The molar ratio of MB2-silane to TMOS is about 1:1000. The solution is left stirring at room temperature overnight. Then, 0.21 mmol of PEG-silane are added and the solution is kept stirring at room temperature overnight. Finally, to promote covalent bond formation between PEG-silane and particles, stirring is stopped and the particle dispersion is heated to 80 °C for 8 hours. To remove any unreacted precursors, aggregates, or dust from the particle dispersion, particles are transferred into a dialysis membrane tube (molecular weight cutoff, MWCO = 10,000), and dialyzed in 2 L of DI water with three water exchanges every 8 hours. After dialysis, the dispersion is subject to syringe filtration (0.2 μm, Fisherbrand) and finally up-concentrated for gel permeation chromatography (GPC) using a membrane spin filter (GE Healthcare, molecular weight cutoff = 30,000) and a centrifuge at 2300 rpm.

3.2.3 Synthesis of Nanophotosensitizers (Design Two)

Particles binding MB2 to the particle surface are synthesized according to the synthesis of design one (excluding the addition of MB2-silane, or replacing MB2 with TMR-maleimide, see main text). MB2 is added to the final silica particles by using the method of post-PEGylation surface modifications by insertion (PPSMI) [8]. To that end, MPTMS is added to the PEGylated particle dispersion under vigorous stirring at a concentration of 2.3 mM. The particle/MPTMS mixture is stirred at room temperature overnight, followed by the addition of $3.67x10^{-7}$ moles MB2-maleimide at a concentration of 37 μM. The solution is vigorously stirred at room temperature for 24 hours for the dye to react with the thiol group on the silica core surface of the particles. Afterwards, the particle dispersion is subjected to the same cleaning process as described before (dialysis, syringe filtration, GPC). Particles containing TMR on the surface were synthesized in the same way by replacing MB2-maleimide with TMR-maleimide.

3.2.4 Targeting Peptide c(RGDyC) Functionalization

Particles were peptide-functionalized with c(RGDyC)-PEG-silane (Supplementary Figure A3). c(RGDyC)-PEG-silane was prepared by exploiting the mercapto group of cysteine of c(RGDyC) (Figure 3D) to click to the maleimide group of a heterobifunctional mal-PEG-NHS first, and then clicking the NHS to the amine group of (3-aminopropyl)trimethoxysilane (APTES). The concentration of NHS ester-PEG-maleimide in DMSO was 0.23 M. The mixed solution was left at room temperature in the glovebox for 3 hours to form silane-PEG-maleimide. After that, c(RGDyC) was added and the solution left at room temperature in the glovebox overnight to produce c(RGDyC)-PEG-silane. The molar ratio c(RGDyC):NHS-PEG-mal:APTES was

1.0:1.0:0.9. In order to functionalize particles with c(RGDyC) peptide ligands, previously prepared c(RGDyC)-PEG-silane was added to the particle dispersion immediately before the addition of PEG-silane. The remainder of the synthesis and purification protocol is as described before.

3.2.5 Gel Permeation Chromatography (GPC)

To remove unreacted precursors from the native particle dispersion, samples were purified using gel permeation chromatography (GPC). A BioLogic LP system with 275 nm UV detector and cross-linked copolymer of allyl dextran and N,N'-methylene bisacrylamide (Sephacryl S-300 HR, GE Healthcare) as solid phase was used. Before GPC purification each sample was up-concentrated with centrifuge spin-filters (Vivaspin with MWCO 30k, GE Healthcare) to an approximate sample volume of 600 µL, run through the column with a 0.9 wt% NaCl solution, and fraction-collected by a BioFrac fraction collector. Sample fractions were transferred to DI water by washing samples five times with centrifuge spin-filters. The resulting particles could be subjected to long-term storage in nitrogen bubbled DI water in the dark at 4 °C.

3.2.6 Steady State Absorption Spectroscopy

Absorbance spectra were measured on a Varian Cary 5000 spectrophotometer. Spectra were measured in DI water using a quartz cuvette (HellmaAnalytics) with a 10 mm light path, and baseline corrected using a second cuvette with pure DI water as a reference cell. All spectra were measured in 1 nm increments and peak intensities were kept between 0.01 and 0.06.

3.2.7 Fluorescence Correlation Spectroscopy (FCS)

A homebuilt confocal FCS setup was used to determine particle hydrodynamic diameter, solution concentration, and number of dye molecules per particle. Particles containing TMR dye were excited with a 543 nm He:Ne laser, that was focused by a water immersion microscope objective (Zeiss Plan-Neofluar 63x NA 1.2). The fluorescence signal passed through a 50 μm pinhole and a long pass filter (ET560lp, Chroma) before being detected by an avalanche photo diode (APD) detector (SPCM-AQR-14, PerkinElmer) and auto-correlated with a digital correlator (Flex03LQ, Correlator.com). Data was fitted using a non-linear least-squares Levenberg-Marquardt algorithm and a triplet corrected correlation function, G(τ), shown in equation (1):

$$G(\tau) = 1 + \frac{1}{N_m}\left(\frac{1}{1+\tau/\tau_D}\right)\left(\frac{1}{1+\tau/(\tau_D\kappa^2)}\right)^{1/2}\frac{1}{(1-T)}(1-T + T\exp(\tau/\tau_T)) \quad (1)$$

Where τ is the lag time, N_m the time- and spaced-averaged number of TMR labeled particles in the FCS observation volume, that is defined by a structure factor $\kappa = \omega_z/\omega_{xy}$ with radial (ω_{xy}) and axial (ω_z) radii. τ_D is the time that a particle takes to diffuse through the observation volume. T is the fraction of TMR molecules being in the triplet state, with a triplet relaxation time, τ_T. FCS correlation curves were normalized using equation (2):

$$G(\tau) = (G(\tau) - 1)\, N_m \quad (2)$$

All samples were measured in 35 mm glass bottom dishes (P35G-1.5-10-C, Mattek Corporation) at nanomolar concentration in DI water at 20 °C, 5 kW cm^{-2} laser power, and in triplets with five 30 s long collection intervals. The observation volume was calibrated before each FCS measurement. Particle diameters, d, were calculated using

the Stokes-Einstein equation (3) with the diffusion constant, D, obtained from equation (4):

$$d = 2\frac{k_B T}{6\pi\eta D} \tag{3}$$

$$D = \frac{\omega_{xy}{}^2}{4\tau_D} \tag{4}$$

The number of TMR or MB2 molecules per particle, n_m, was determined by comparing the dye concentration from steady state absorption spectroscopy, C_{Abs}, and the particle concentration measured in FCS, $\langle C \rangle_{FCS}$, using equation (5):

$$n_m = \frac{C_{Abs}}{\langle C \rangle_{FCS}} \tag{5}$$

where it was assumed that the molar extinction coefficients do not change upon dye encapsulation.

3.2.8 Determination of Singlet Oxygen Quantum Yields, Φ_Δ

Singlet oxygen quantum yield, Φ_Δ, measurements were carried out in ethanol with 1,3-diphenylisobenzofuran (DPBF) as a detector molecule for trapping singlet oxygen. The generation of singlet oxygen could be observed by a reduction of the DPBF absorption band at 410 nm (Figure 5A). Measurements were carried out at sample optical densities of 0.15 – 0.50 in a 100 µL quartz cuvette (Starna). Samples were evenly exposed to a 635 nm, expanded, and collimated laser beam of a solid-state laser (Power Technology Inc.) at 3 mW/cm^2 with a spot size of about 1 cm in the same cell. To acquire a 0.5 - 0.6 absorption, DPBF was added at a concentration of approximately 18.75 µM. All absorption spectra were measured in 1 nm steps and baseline-corrected against a second cuvette with ethanol as a reference cell. The sample absorption was

recorded at defined time intervals and corrected for the sample absorption spectrum in the absence of DPBF. Φ_Δ was calculated by comparing all samples to the standard methylene blue (MB) dye with known singlet oxygen quantum yield of $\Phi_\Delta = 0.52$ (in ethanol) [39] by plotting the natural logarithm of the reduction of the 410 nm DBPF band against the exposure time and using equation (6), where m represents the slope of a linear fit through the data points (Figure 5B):

$$\Phi_\Delta(sample) = \Phi_\Delta(MB)\frac{m(sample)}{m(MB)} \quad (6)$$

To determine the effective singlet oxygen quantum yield, Φ_Δ^{eff}, the particle concentration as determined by FCS and the MB concentration were matched.

3.3 Results and Discussion

Silica nanophotosensizers (SNPSs) covalently encapsulating the methylene blue derivate MB2 inside the particle (design one, Figure 3C) were synthesized by combining tetramethylorthosilcate (TMOS) and MB2-silane (Figure 3B) in basic aqueous solution. After particle formation, further particle growth was quenched by the addition of PEG-silane (Figure 3B) to the reaction mixture. Particles containing MB2 on the particle surface (design two, Figure 3C) were synthesized in the same way, however, MB2 was attached using a grafting method referred to as post-PEGylation surface modification by insertion (PPSMI) [8]. This method employs amine-reactive or sulfhydryl-reactive click chemistry, by adding amine-silanes or thiol-silanes, respectively, below the nucleation threshold into an aqueous dispersion of PEGylated SNPs. The small molar mass silane precursors diffuse through the PEG corona chains and react with the silica

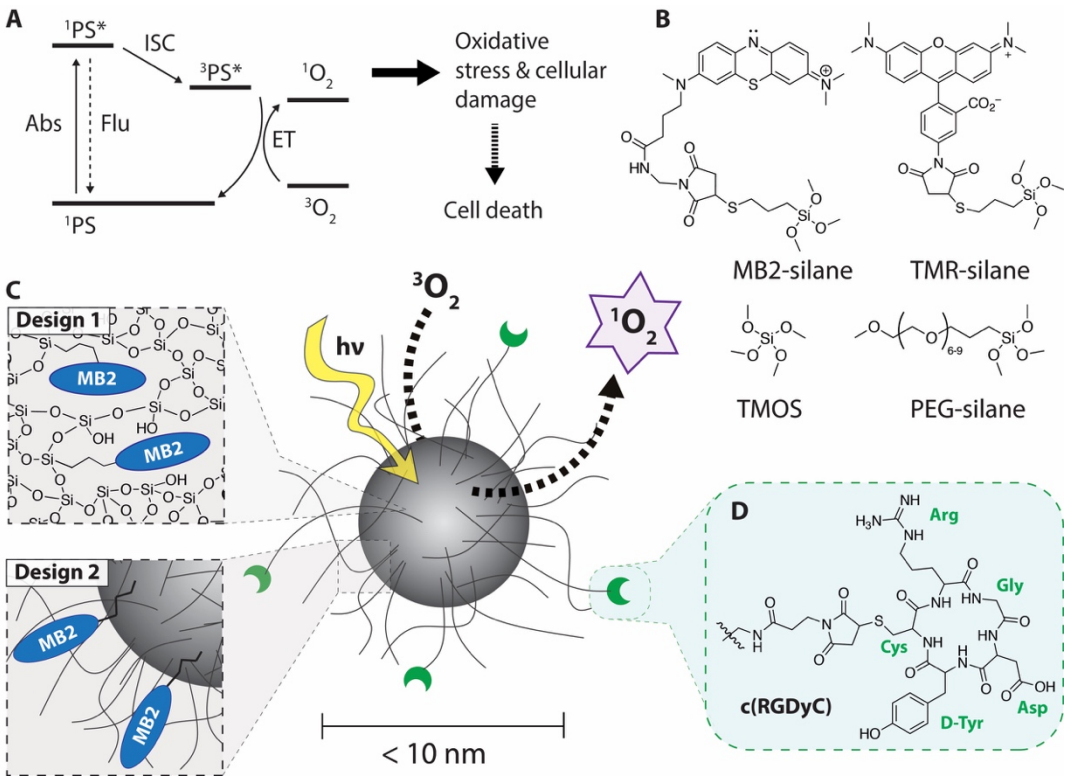

Figure 3. (A) Simplified Jablonski Scheme illustrating the creation of reactive singlet oxygen, $^1O_2$. ^{1}PS denotes the singlet ground state, ^{1}PS* the electronically excited singlet state, and ^{3}PS* the electronically excited triplet state of a photosensitizer. $^3O_2$ denotes the triplet ground state of molecularly dissolved oxygen. (B) Precursor molecules for the synthesis of sub-10 nm silica nanoparticles, showing the MB2-silane, the rhodamine dye TMR-silane, tetramethyl orthosilicate (TMOS), and polyethylene glycol-silane (PEG-silane). (C) Schematic representation of two different designs of functionalized photosensitizing sub-10 nm silica nanoparticles (center). Design 1: Covalent encapsulation of one or more MB2 molecules in the silica matrix (PEG-MB2-C' dots). Design 2: Particle surface functionalization with one or more MB2 molecules (MB2-PEG-C'dot). (D) Targeting moiety cyclo(Arg-Gly-Asp-D-Tyr-Cys) (cRGDyC).

particle surface. The pending amine or thiol groups can further be reacted with N-hydroxysuccinimide or maleimide functional groups, respectively [8]. For design two, we used (3-mercaptopropyl)trimethoxysilane (MPTMS) to functionalize the particle surface with thiol groups to click MB2-maleimide to the particle (for details see Section 3.2.3). Finally, all particles were cleaned from unreacted precursors via gel permeation chromatography (GPC) prior to further characterization.

Due to the weakly-emissive nature of MB2 (Supplementary Figure A2), fluorescence-based size determination of MB2 functionalized particles by fluorescence correlation spectroscopy (FCS) was not possible. To make particle samples accessible for the determination of hydrodynamic diameters and particle concentrations by FCS, particles were further functionalized with the fluorescent dye tetramethylrhodamine-silane (TMR-silane) (Figure 3B). For design one we grafted TMR onto the particle surface using PPSMI and for design two we synthesized SNPs encapsulating TMR dye before MB2 was grafted on the particle surface. A combination of FCS and steady state absorption spectroscopy was used to determine the number of MB2 and TMR molecules per particle. Particle diameter and concentration were determined by measuring the fluorescence fluctuations of particles diffusing through a well-defined observation volume of a laser beam and subsequently auto-correlating the fluorescence time signal. The resulting FCS correlation curves were fitted with a correlation function (see equation (1), Section 3.2.7) from which the time averaged number of particles and the diffusion constant were extracted. To determine the number of dyes per particle, the dye concentration as determined by steady-state absorption spectroscopy was compared to the concentration of the particles as determined by FCS (equation (5), Section 3.2.7),

yielding the average number of dyes per particle. For accurately determining the number of MB2 dyes per particle, it is necessary that every MB2 containing particle carries at least one TMR dye, a requirement that is not necessarily met. We accounted for that to the best possible degree by working with high concentrations of TMR. Dye molecules that were not covalently bound during synthesis were washed away by dialysis and separated from the particles by GPC. Supplementary Figure A4A and A4B show the GPC chromatograms before and after TMR and MB2 surface functionalization of particles, respectively. Both chromatogram-pairs show a single peak and were congruent to each other, indicating that TMR dye molecules (design one), or MB2 dye molecules (design two) were grafted onto the respective SNPs.

Figure 4A and 4B show the FCS correlation curves of the fluorescent particles. The curves were fitted using a triplet corrected translational diffusion correlation function (equation (1), Section 3.2.7). Particle hydrodynamic diameters of 5.9 nm for MB2 encapsulating C' dots with TMR surface functionalization (TMR-PEG-MB2-C' dots), 5.2 nm for TMR encapsulating C' dots (PEG-TMR-C' dots), and 5.2 nm for TMR encapsulating C' dots with MB2 surface functionalization (MB2-PEG-TMR-C' dots) were obtained (a comprehensive nomenclature to describe C' dots is described in the supporting information of reference [8]). Figure 4C and 4D show the UV-vis absorption spectra of PEG-MB2-C' dots, TMR-PEG-MB2-C' dots, PEG-TMR-C' dots, and MB2-PEG-TMR-C' dots in water, respectively. For comparison, the absorption spectra of TMR-maleimide and MB2-maleimide are superimposed onto the particle spectra. For TMR-PEG-MB2-C' dots and MB2-PEG-TMR-C' dots, a TMR absorption

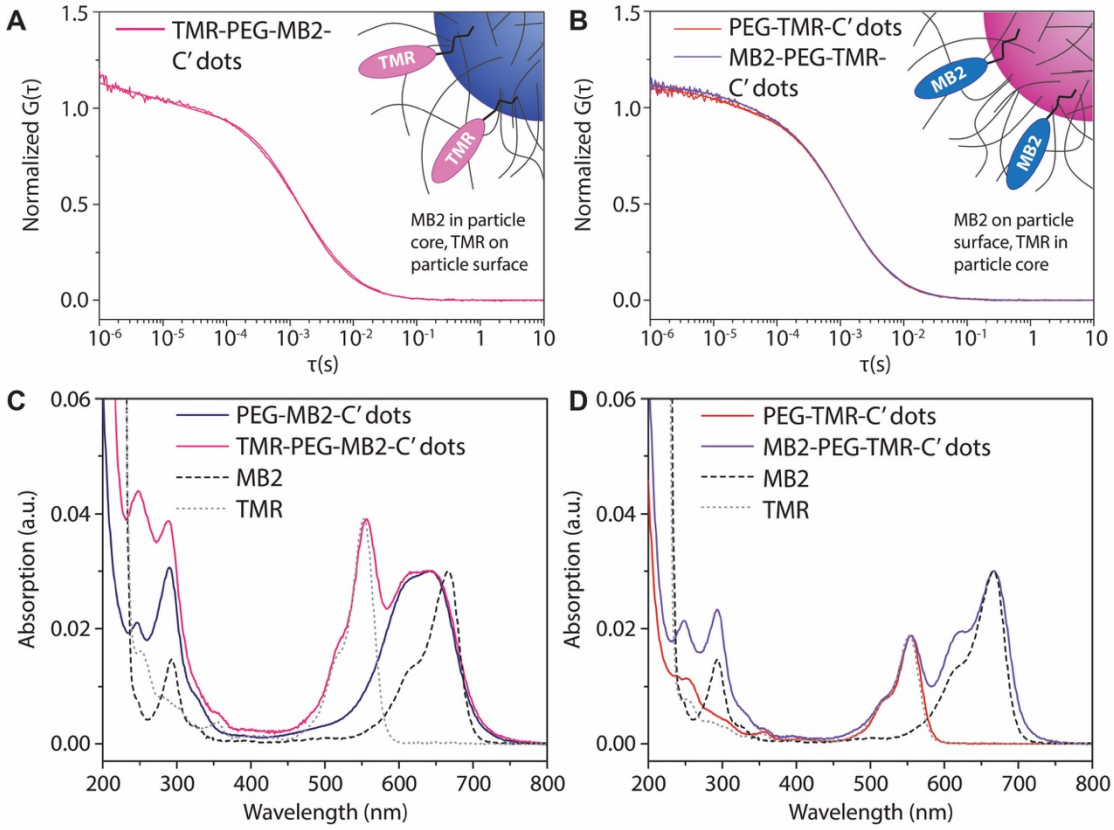

Figure 4. (A) and (C) FCS autocorrelation curve of MB2-PEG-TMR-C'dot (design one) and absorption spectra before and after TMR surface functionalization as compared to free TMR dye and MB2 photosensitizer. (B) and (D) FCS autocorrelation curves of PEG-TMR-C' dots and TMR-PEG-MB2-C' dots (design two) and absorption spectra before and after MB2 surface functionalization as compared to free TMR dye and MB2 photosensitizer.

peak can be observed indicating successful functionalization of particles with TMR and MB2, respectively.

Comparing the absorption profiles of MB2 for the two different designs, a relative hypsochromic shift (blue-shift) from 668 nm to 644 nm of the main peak for design one relative to free MB2 is observed that is absent in design two. This hypsochromic shift likely originates from dimethylation of the auxochrome groups of MB2, from $-N(CH_3)_2$ to $-NH(CH_3)$ and/or $-NH_2$, which is promoted in basic media [40][41]. In addition, both designs display a heightened left shoulder in the absorption peak as compared to free MB2 dye that is more pronounced in design one than it is in design two. The heightened shoulders around 620 nm and 605 nm for design two and one, respectively, are a result of dimerization of MB2 at high concentrations (1×10^{-6} to 4×10^{-4} M) in aqueous media (MB2 concentrations during synthesis is $3.67x10^{-5}$ M) [42]. Methylene blue monomers and dimers are known to have distinct absorption peaks located at 664 nm and 590 nm, respectively, with an equilibrium constant of $3.8x10^{3}$ M^{-1} in water [43]. However, the formation of dimers is not only dependent on concentration but is additionally promoted by the presence of oppositely charged surfaces [44]. For design one, the cationic MB2 photosensitizer was added to the synthesis during the silica particles formation and hence was exposed to negatively charged silica nucleation seeds (at pH 9). For design two, MB2 was grafted onto the PEGylated silica particle surface at neutral conditions (pH 7), consequently showing no peak shift and relatively fewer MB2 dimers, despite the same MB2 concentration during the synthesis as for design one.

To determine the number of MB2 molecules per particle we compared the particle concentrations estimated by FCS and the MB2 concentrations from steady-state absorption measurements. For practical reasons, we assumed that the extinction coefficient remained unaffected in the particle synthesis. This is not necessarily true due to the metachromatic nature of methylene blue and demethylation. Based on this assumption we estimated the average number of dyes per particle (equation (5), Section 3.2.7) to be 2.4/3.3 for MB2/TMR for design one and 3.4/2.3 for MB2/TMR for design two.

Next, we measured the singlet oxygen quantum yield, Φ_Δ, for both particle designs using the singlet oxygen sensor 1,3-diphenylisobenzofuran (DPBF). For these measurements, we matched the particle concentrations as determined by FCS to yield an effective singlet oxygen quantum yield per SNPS (Φ_Δ^{eff} (SNPS)). Figure 5A demonstrates the principle of oxygen sensing using DPBF and the particle TMR-PEG-MB2-C' dots (design one) in ethanol. The mixture is evenly exposed to an expanded and collimated 635 nm laser beam for defined time intervals. The singlet oxygen that is generated by the SNPSs reacts with DPBF molecules, yielding 1,2-dibenzoylbenzene [45]. The formation of 1,2-dibenzoylbenzene was monitored via a reduction of the absorption band at 410 nm. By comparing samples to a methylene blue standard (Φ_Δ(MB) = 0.52), Φ_Δ^{eff}(SNPS) was determined (see equation (6), Section 3.2.7), resulting in values of 111% for design one (TMR-PEG-MB2-C' dots) and 161% for design two (MB2-PEG-TMR-C' dots). This translates to an estimated per dye singlet oxygen quantum yield of 46% and 47%, respectively, based on the estimated number of MB2 dyes per particle. The relatively lower values for Φ_Δ of the dyes associated with

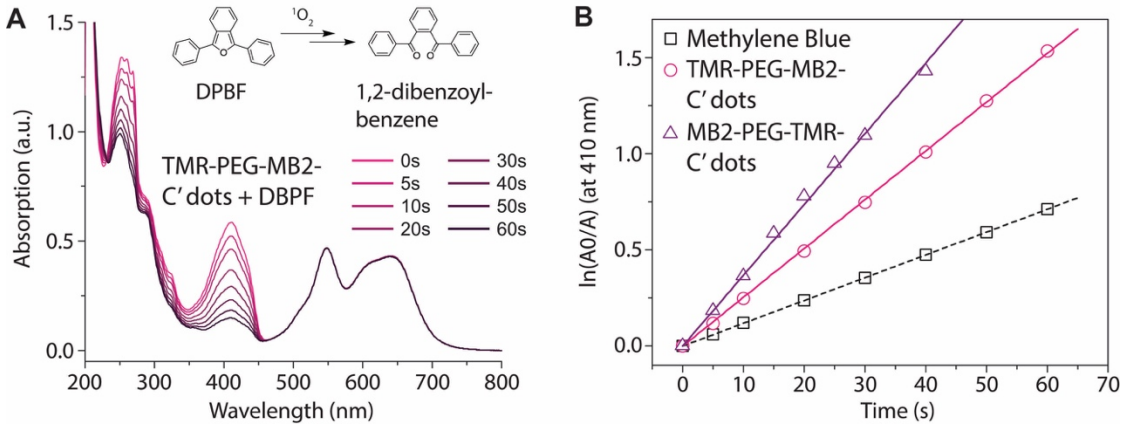

Figure 5. (A) Schematic representation of a photosensitizing measurement using 1,3-diphenylisobenzofuran (DPBF) as a singlet oxygen, $^1O_2$, sensor. Absorption of a solution containing TMR-PEG-MB2-C' dots and DPBF irradiated at 635 nm for 60 s in intervals of 5 s (see legend). (B) Comparative $^1O_2$ generation of methylene blue, TMR-PEG-MB2-C' dots, and MB2-PEG-TMR-C' dots.

the particles versus free methylene blue dye can be rationalized by the steric shielding effects of encapsulation or grafting within the PEGylation corona. The silica network and/or the PEG molecules shield diffusing oxygen, first, from MB2, and then, from DPBF resulting in a reduced singlet oxygen quantum yield. Although for both designs the per dye Φ_Δ values are similar, surface grafted MB2 molecules are likely less shielded than dyes fully encapsulated in the silica network. In addition, it is known that methylene blue dimers and monomers engage in different photochemical processes. While monomers undergo energy transfer reaction with triplet oxygen, dimers engage in electron transfer reactions with other methylene blue molecules [43]. These different energy dissipation pathways of dimers correlate negatively with the singlet oxygen quantum yield contributing to the reduced singlet oxygen quantum yield per dye molecule of design one and design two [46]. However, the multiplicity effect stemming from multiple MB2 molecules colocalized on one particle compensates for a reduced per dye singlet oxygen quantum yield by steric shielding and/or dimerization.

To exclude the possibility of $^1O_2$ formation in the absence of irradiation with light (dark toxicity) for the different particle designs, we repeated singlet oxygen quantum yield measurements, but did not expose the samples to the laser beam. Supplementary Figure A5 shows results of the same experiment as shown in Figure 5A for design one (PEG-MB2-C' dots). This time, the DPBF peak at 410 nm remains unchanged, however, indicating no formation of 1,2-dibenzoylbenzene and hence no generation of singlet oxygen. This is the case for both designs.

Specific targeting of photosensitizers to diseased tissue increases the efficacy of PDT and minimizes collateral damage to healthy tissue. We therefore functionalized

SNPSs with the targeting moiety cyclo(arginine-glycine-aspartic acid-D-tyrosine-cysteine) (c(RGDyC)) (Figure 3C), which targets $\alpha_v\beta_3$ integrins overexpressed, e.g. on various cancer cells including melanoma [33]. It has been shown that the endocytosis-mediated cellular uptake of c(RGDyC) functionalized particles correlates with the $\alpha_v\beta_3$-expression levels of cells [47][48], and increases the intracellular particle concentration, rendering c(RGDyC) a specific targeting moiety with high affinity for the treatment of the melanoma cancer [23][49].

Particles were functionalized by adding c(RGDyC)-PEG-silane (Supplemenatry Figure A3A) during the PEGylation step (for details see Section 3.2.4) [34]. To allow more steric freedom for ligand binding to integrins, the c(RGDyC)-PEG-silane was chosen to be three ethylene oxide (EO) units longer than the PEG-silane (twelve versus six-nine units). Due to the weakly-fluorescent nature of MB2, an FCS analysis could not be conducted. Instead we compared the GPC chromatograms before and after peptide functionalization for particle design one (PEG-MB2-C' dots and c(RGDyC)-PEG-MB2-C' dots), and two (MB2-PEG-C' dots and MB2-c(RGDyC)-PEG-C' dots) (Supplementary Figures A6A and A6B). In both cases, we observed single peaks that were congruent to each other. All particles were then characterized using steady-state absorption spectroscopy. Figure 6A and 6D show the absorption spectra of design one and design two, respectively, with and without c(RGDyC)-functionalization in water. In both cases, increased absorption between 200 and 300 nm was noticeable. Due to strong absorption features in that region it is difficult to clearly identify the peptide absorption by qualitative comparison. For that reason, we deconvoluted the two spectra and display the difference spectra in Figures 6B and 6E. In both cases a band at ~260 to

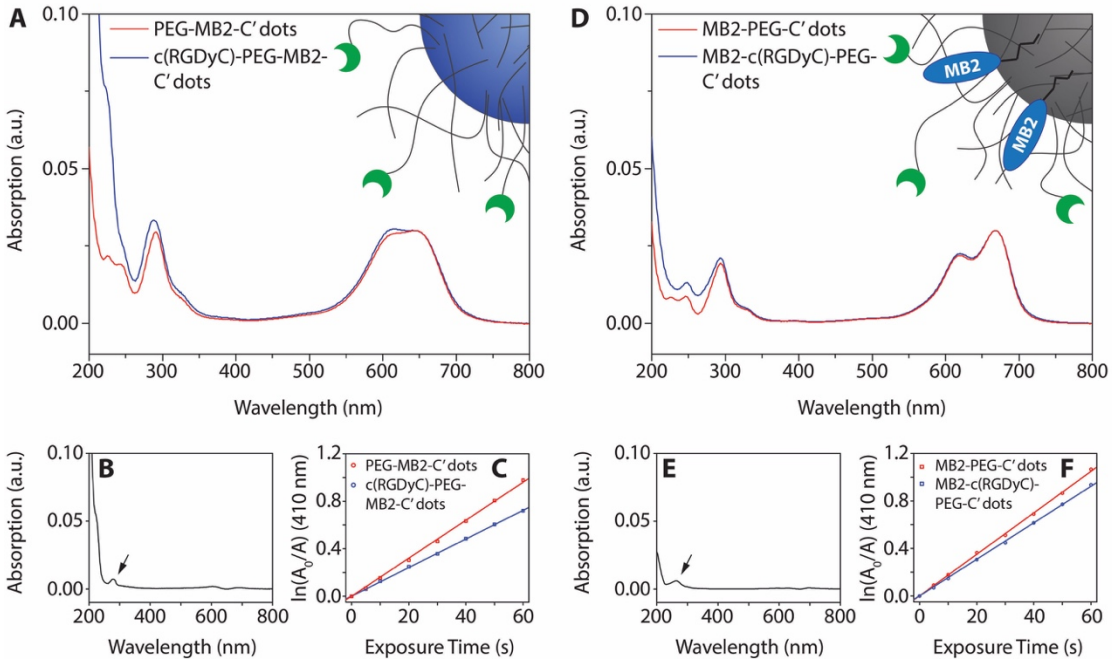

Figure 6. (A) Intensity matched absorption spectra of PEG-MB2-C' dots and c(RGDyC)-PEG-MB2-C' dots. (B) Difference spectrum of the spectra in (A). (C) Photosensitizing measurement of intensity matched PEG-MB2-C' dots and c(RGDyC)-PEG-MB2-C' dots. (D) Intensity matched absorption spectra of MB2-PEG-C' dots and MB2-c(RGDyC)-PEG-C' dots. (E) Difference spectrum of the spectra in (D). (F) Photosensitizing measurement of intensity matched MB2-PEG-C' dots and MB2-c(RGDyC)-PEG-C' dots.

270 nm can clearly be identified, which coincides with the absorption band of the c(RGDyC) spectrum (Supplementary Figures A6C). Using the relative absorption peaks of tyrosine in c(RGDyC) and of MB2, we estimated 17 and 14 c(RGDyC) units per MB2 molecule for design one and design two, respectively, which is close to the desired number based on earlier studies [49].

Finally, we tested the effect of c(RGDyC)-functionalization on the relative singlet oxygen quantum yield performance. We compared particles with and without c(RGDyC) for absorption matched samples of the same design. For both designs we measured a reduction of singlet oxygen quantum yield by a relative 25% for design one and by a relative 12% for design two (Figure 6C and 6F). This finding is surprising. Given the spatial proximity of surface MB2 and c(RGDyC), one would expect a stronger effect of c(RGDyC) in design two. Results suggest, however, that c(RGDyC) increases the steric shielding more significantly for the encapsulated MB2 than for the surface grafted MB2.

3.4 Contributions

Chapter 2 and 3 of this thesis are based on the manuscript named 'Designing PEGylated and Functionalized Sub-10 nm Silica Methylene Blue Nanophotosensitizers' with co-first authorship between Ferdinand F. E. Kohle and me. F. F. E. Kohle and I synthesized nanoparticles and conducted steady-state absorption and emission spectroscopy. F. F. E. Kohle helped me with analysis of steady-state absorption and emission spectroscopy and conducted FCS measurements. F. F. E. Kohle and I carried out singlet oxygen quantum yield measurements.

CHAPTER 4

CONCLUSIONS AND FUTURE WORK

4.1 Conclusions

In this thesis, we have presented the synthesis of two different designs for ultrasmall organic-inorganic hybrid silica nanophotosenistizers, that covalently bind the methylene blue derivate MB2. We found that the properties of MB2 strongly depend on the particle design. Both particle designs yielded sub-10 nm size particles that could be functionalized with c(RGDyC) as a targeting moiety. Despite reduced singlet oxygen quantum yields of MB2 upon particle association, the effective particle singlet oxygen quantum yields far exceed the quantum yield of a single MB2 dye. The advantages of ultrasmall organic-inorganic hybrid functionalized silica nanoparticles as a delivery and protective system for photosensitizers make such probes interesting candidates for applications in PDT.

4.2 Future Work

Although this thesis focuses on the photosensitizer MB2, described design principles and synthesis methods are in principle applicable to other photosensitizers. This might be of special interest for hydrophobic NIR and IR photosensitizers with large singlet oxygen quantum yields, *i.e.* porphyrins, chlorins, phthalocyanines, naphthalocyanines, bacteriochlorins, and BODIPY dyes. PEGylated silica can provide a water-soluble carrier for these cargos, to allow specific targeting and achieve high local concentrations at targeted sites, while avoiding aggregation in aqueous media.

However, more work is necessary to fine tune such synthesis protocols to fully harvest the potential of ultrasmall organic-inorganic hybrid silica nanophotosenistizers. Moreover, subsequent *in vitro* and *in vivo* experiments are required for practical PDT applications to test the singlet oxygen quantum yield of SNPSs in cells, which will offer guidelines to potential clinical translations in the future.

APPENDIX

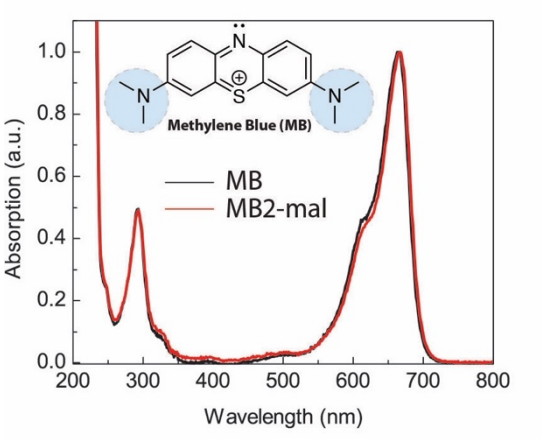

Figure A1. Methylene blue (MB) and MB2 absorption spectra. A minor bathochromic shift (red-shift) from 665 to 667 nm is noticeable. The inset shows the chemical structure of MB with auxochrome groups circled in blue.

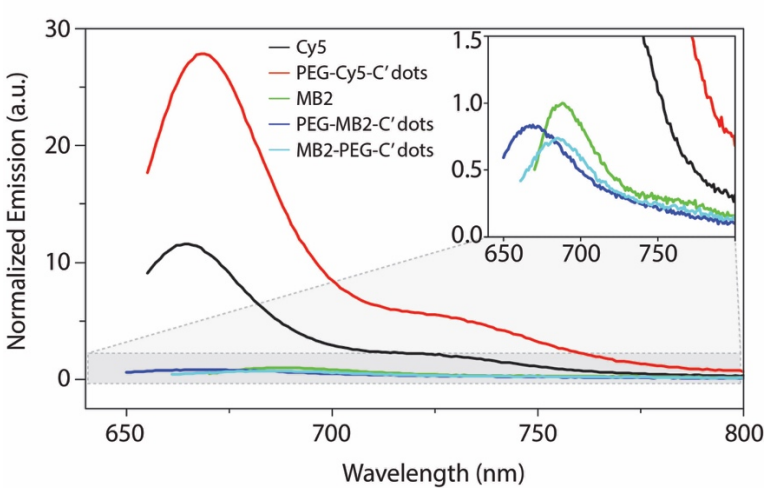

Figure A2. Fluorescence emission spectra of Cy5 dye, PEG-Cy5-C' dots, MB2, PEG-MB2-C' dots, and MB2-PEG-C' dots. The concentration of Cy5 and MB2 was matched. The emission spectra were normalized for the emission of MB2. The inset shows the

enlarged emission of MB2, PEG-MB2-C' dots, and MB2-PEG-C' dots, showing a more than one order of magnitude brightness difference between the Cy5 and PEG-Cy5-C' dots and MB2, PEG-MB2-C' dots, and MB2-PEG-C' dots. Cy5 particles show the typical emission enhancement that is observed upon dye encapsulation in a silica matrix as compared to the free dye in solution [50] [51]. The emission of PEG-MB2-C' dots as compared to MB2-PEG-C' dots is slightly larger, however both particles demonstrate a reduction of emission as compared to free MB2. This can likely be associated with the increased shoulder of MB2 in the particles.

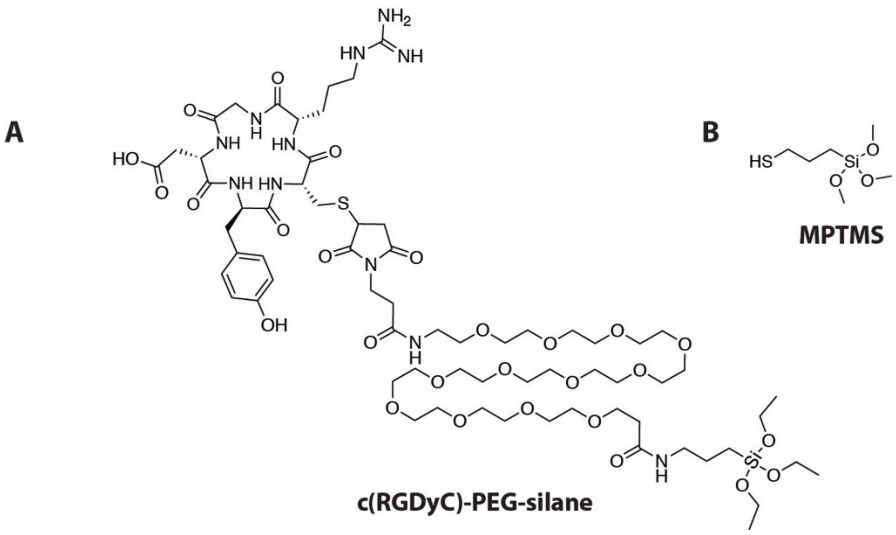

Figure A3. (A) Chemical structure of the targeting moiety precursor (cRGDyC)-PEG(12)-silane. (B) Chemical structure of (3-mercaptopropyl)trimethoxysilane (MPTMS).

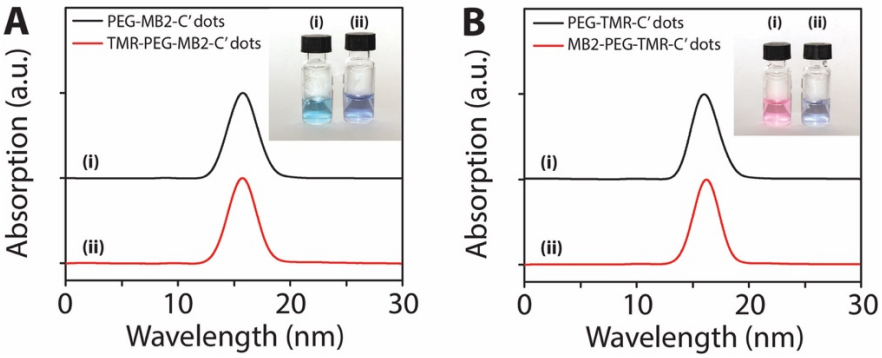

Figure A4. (A) GPC elugrams of PEG-MB2-C' dots (i) and TMR-PEG-MB2-C' dots (ii). Inset shows photographs of the respective samples. (B) GPC elugrams of PEG-TMR-C' dots (i) and MB2-PEG-TMR-C' dots (ii). Inset shows photographs of the respective samples. Each sample pair was measured on the same day. Different sample pairs were measured on different days leading to differences in absolute peak elution times.

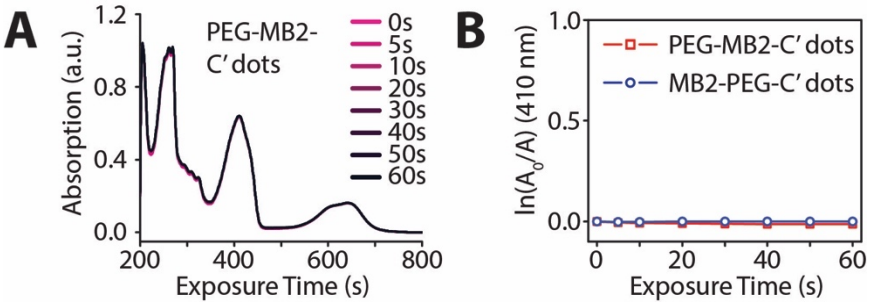

Figure A5. (A) Schematic representation of a photosensitizing measurement using 1,3-diphenylisobenzofuran (DPBF) as a singlet oxygen, $^1O_2$, sensor. Absorption of a solution containing PEG-MB2-C' dots and DPBF, measured at different time points, in the absence of 635 nm irradiation (dark toxicity). (B) Comparison of singlet oxygen, $^1O_2$, generation from PEG-MB2-C' dots and MB2-PEG-C' dots in the dark.

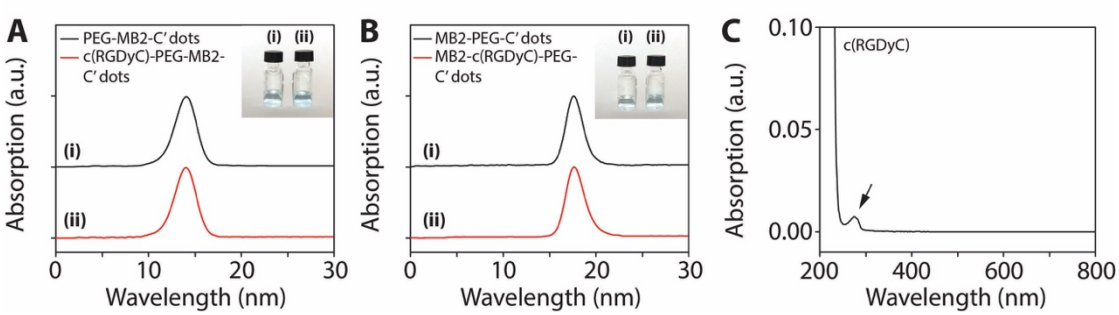

Figure A6. (A) GPC elugrams of PEG-MB2-C' dots (i) and c(RGDyC)-PEG-MB2-C' dots (ii). Inset shows photographs of the respective samples. (B) GPC elugrams of MB2-PEG-C' dots (i) and MB2-c(RGDyC)-PEG-C' dots (ii). Inset shows photographs of the respective samples. Each sample pair was measured on the same day. Different sample pairs were measured on different days leading to differences in absolute peak elution times. (C) Absorption spectrum of c(RGDyC) in water, showing an isolated tyrosin peak ($\varepsilon \approx 1400\ M^{-1}\ cm^{-1}$) [34].

REFERENCES

(1) Felsher, D. W. Photodynamic Therapy for Cancer. *Nat. Rev. Cancer* **2003**, *3*, 375–380.

(2) Daniell, M. D. & Hill, J. S. A history of photodynamic therapy. *Aust. NZ J. Surg*. **1991**, *61*, 340–3482.

(3) Meyer–Betz, F. Untersuchungen uber die biologische photodynamische Wirkung des Hematoporphyrins und anderer Derivative des Blut und Galenafarbstoffs. *Dtsch Arch. Klin*. **1913**, *112*, 476–503.

(4) Lipson, R. L. & Baldes, E. J. The photodynamic properties of a particular hematoporphyrin derivative. *Arch. Dermatol*. **1960**, *82*, 508–516.

(5) Lipson, R. L., Baldes, E. J. & Olsen, A. M. The use of an derivative of hematoporphyrin in tumor detection. *J. Natl Cancer Inst*. **1961**, *26*, 1–11.

(6) Dougherty, T. J., Grindey, G. B., Fiel, R., Weishaupt, K. R. & Boyle, D. G. Photoradiation therapy. II. Cure of animal tumors with hematoporphyrin and light. *J. Natl Cancer Inst.* **1975**, *55*, 115–121.

(7) Abrahamse, H.; Kruger, C. A.; Kadanyo, S.; Mishra, A. Nanoparticles for Advanced Photodynamic Therapy of Cancer. *Photomed. Laser Surg.* **2017**, *35*, 581-588.

(8) Ma, K.; Wiesner, U. Modular and Orthogonal Post-PEGylation Surface Modifications by Insertion Enabling Penta-Functional Ultrasmall Organic-Silica Hybrid Nanoparticles. *Chem. Mater.* **2017**, *29*, 6840–6855.

(9) *PROVAYBLUETM (methylene blue) injection, for intravenous use*; U.S. Food and Drug Administration, **2016**.

(10) Tardivo, J. P.; Giglio, A. Del; Santos De Oliveira, C.; Santesso Gabrielli, D.; Couto Junqueira, H.; Tada, D. B.; Severino, D.; De Fátima Turchiello, R.; Baptista Phd, M. S. Methylene Blue in Photodynamic Therapy: From Basic Mechanisms to Clinical Applications. *Photodiagnosis Photodyn. Ther.* **2005**, *2*, 175–191.

(11) Tang, W.; Xu, H.; Park, E. J.; Philbert, M. A.; Kopelman, R. Encapsulation of Methylene Blue in Polyacrylamide Nanoparticle Platforms Protects Its Photodynamic Effectiveness. *Biochem. Biophys. Res. Commun.* **2008**, *369*, 579–583.

(12) Tang, W.; Xu, H.; Kopelman, R.; A. Philbert, M. Photodynamic Characterization and In Vitro Application of Methylene Blue-Containing Nanoparticle Platforms. *Photochem. Photobiol.* **2005**, *81*, 242.

(13) Qin, M.; Hah, H. J.; Kim, G.; Nie, G.; Lee, Y.-E. K.; Kopelman, R. Methylene Blue Covalently Loaded Polyacrylamide Nanoparticles for Enhanced Tumor-Targeted Photodynamic Therapy. *Photochem. Photobiol. Sci.* **2011**, *10*, 832–841.

(14) Ochsner, M. Photophysical and Photobiological Processes in the Photodynamic Therapy of Tumours. *J. Photochem. Photobiol. B Biol.* **1997**, *39*, 1–18.

(15) DeRosa, M. C.; Crutchley, R. J. Photosensitized Singlet Oxygen and Its Applications. *Coord. Chem. Rev*. **2002**, *233–234*, 351–371.

(16) Ormond, A. B.; Freeman, H. S. Dye Sensitizers for Photodynamic Therapy.

Materials. **2013**, *6*, 817–840.
(17) Agostinis, P.; Berg, K.; Cengel, K. a; Foster, T. H.; Girotti, A. W.; Gollnick, S. O.; Hahn, S. M.; Hamblin, M. R.; Juzeniene, A.; Kessel, D.; Korbelik, M.; Moan, J.; Mroz, P.; Nowiz, D.; Piette, J.; Willson, B. C.; Golab, J. Photodynamic Therapy of Cancer : An Update. *Am. Cancer Soc.* **2011**, *61*, 250–281.
(18) Mehraban, N.; Freeman, H. S. Developments in PDT Sensitizers for Increased Selectivity and Singlet Oxygen Production. *Materials*. **2015**, *8*, 4421-4456.
(19) Kamkaew, A.; Lim, S. H.; Lee, H. B.; Kiew, L. V.; Chung, L. Y.; Burgess, K. BODIPY Dyes in Photodynamic Therapy. *Chem. Soc. Rev. Chem. Soc. Rev.* **2013**, *42* (42), 77–88.
(20) Zhang, Y.; Lovell, J. F. Porphyrins as Theranostic Agents from Prehistoric to Modern Times. *Theranostics.* **2012**, *2*, 905–915.
(21) Tang, W.; Xu, H.; Park, E. J.; Philbert, M. A.; Kopelman, R. Encapsulation of Methylene Blue in Polyacrylamide Nanoparticle Platforms Protects Its Photodynamic Effectiveness. *Biochem. Biophys. Res. Commun.* **2008**, *369*, 579–583.
(22) Singh, R.; Lillard, J. W. Nanoparticle-Based Targeted Drug Delivery. *Exp. Mol. Pathol.* **2009**, *86*, 215–223.
(23) Chen, F.; Ma, K.; Zhang, L.; Madajewski, B.; Zanzonico, P.; Sequeira, S.; Gonen, M.; Wiesner, U.; Bradbury, M. S. Target-or-Clear Zirconium-89 Labeled Silica Nanoparticles for Enhanced Cancer-Directed Uptake in Melanoma: A Comparison of Radiolabeling Strategies. *Chem. Mater.* **2017**, *29*, 8269–8281.
(24) Soo Choi, H.; Liu, W.; Misra, P.; Tanaka, E.; Zimmer, J. P.; Itty Ipe, B.; Bawendi, M. G.; Frangioni, J. V. Renal Clearance of Quantum Dots. *Nat. Biotechnol.* **2007**, *25*, 1165–1170.
(25) Debele, T. A.; Peng, S.; Tsai, H. C. Drug Carrier for Photodynamic Cancer Therapy. *Int. J. Mol. Sci.* **2015**, *16*, 22094-22136.
(26) Lucky, S. S.; Soo, K. C.; Zhang, Y. Nanoparticles in Photodynamic Therapy. *Chem. Rev.* **2015**, *115*, 1990–2042.
(27) Gupta, A.; Avci, P.; Sadasivam, M.; Chandran, R.; Parizotto, N.; Vecchio, D.; de Melo, W. C. M. A.; Dai, T.; Chiang, L. Y.; Hamblin, M. R. Shining Light on Nanotechnology to Help Repair and Regeneration. *Biotechnol. Adv.* **2013**, *31*, 607–631.
(28) Chouikrat, R.; Seve, A.; Vanderesse, R.; Benachour, H.; Barberi-Heyob, M.; Richeter, S.; Raehm, L.; Durand, J.-O.; Verelst, M.; Frochot, C. Non Polymeric Nanoparticles for Photodynamic Therapy Applications: Recent Developments. *Curr. Med. Chem.* **2012**, *19*, 781–792.
(29) Ragelle, H.; Danhier, F.; Préat, V.; Langer, R.; Anderson, D. G. Nanoparticle-Based Drug Delivery Systems: A Commercial and Regulatory Outlook as the Field Matures. *Expert Opin. Drug Deliv.* **2017**, *14*, 851–864.
(30) Bobo, D.; Robinson, K. J.; Islam, J.; Thurecht, K. J.; Corrie, S. R. Nanoparticle-Based Medicines: A Review of FDA-Approved Materials and Clinical Trials to Date. *Pharm. Res.* **2016**, *33*, 2373–2387.
(31) Lismont, M.; Dreesen, L.; Wuttke, S. Metal-Organic Framework Nanoparticles in Photodynamic Therapy: Current Status and Perspectives. *Adv. Funct. Mater.*

2017, *27*, 1–16.
(32) Burns, A. a; Vider, J.; Ow, H.; Herz, E.; Penate-medina, O.; Baumgart, M.; Larson, S. M.; Wiesner, U.; Bradbury, M. Fluorescent Silica Nanoparticles with Efficient Urinary Excretion for Nanomedicine. *Nano Lett.* **2009**, *9*, 442–448.
(33) Phillips, E.; Penate-Medina, O.; Zanzonico, P. B.; Carvajal, R. D.; Mohan, P.; Ye, Y.; Humm, J.; Gonen, M.; Kalaigian, H.; Schoder, H.; Strauss, H. W.; Larson, S. M.; Wiesner, U.; Bradbury, M. S. Clinical Translation of an Ultrasmall Inorganic Optical-PET Imaging Nanoparticle Probe. *Sci. Transl. Med.* **2014**, *6*, 260ra149.
(34) Ma, K.; Mendoza, C.; Hanson, M.; Werner-Zwanziger, U.; Zwanziger, J.; Wiesner, U. Control of Ultrasmall Sub-10 Nm Ligand-Functionalized Fluorescent Core-Shell Silica Nanoparticle Growth in Water. *Chem. Mater.* **2015**, *27*, 4119–4133.
(35) Ma, K.; Werner-Zwanziger, U.; Zwanziger, J.; Wiesner, U. Controlling Growth of Ultrasmall Sub-10 Nm Fluorescent Mesoporous Silica Nanoparticles. *Chem. Mater.* **2013**, *25*, 677–691.
(36) Kim, S. E.; Zhang, L.; Ma, K.; Riegman, M.; Chen, F.; Ingold, I.; Conrad, M.; Turker, M. Z.; Gao, M.; Jiang, X.; Monette, S.; Pauliah, M.; Gonen, M.; Zanzonico, P.; Quinn, T.; Wiesner, U.; Bradbury, M. S.; Overholtzer, M. Ultrasmall Nanoparticles Induce Ferroptosis in Nutrient-Deprived Cancer Cells and Suppress Tumour Growth. *Nat. Nanotechnol.* **2016**, *11*, 977–985.
(37) Tang, W.; Xu, H.; Kopelman, R.; A. Philbert, M. Photodynamic Characterization and In Vitro Application of Methylene Blue-Containing Nanoparticle Platforms. *Photochem. Photobiol.* **2005**, *81*, 242.
(38) Qin, M.; Hah, H. J.; Kim, G.; Nie, G.; Lee, Y.-E. K.; Kopelman, R. Methylene Blue Covalently Loaded Polyacrylamide Nanoparticles for Enhanced Tumor-Targeted Photodynamic Therapy. *Photochem. Photobiol. Sci.* **2011**, *10*, 832–841.
(39) Redmond, R. W.; Gamlin, J. N. A Compilation of Singlet Oxygen Yields from Biologically Relevant Molecules. *Photochem. Photobiol.* **1999**, *70*, 391–475.
(40) Yogi, C.; Kojima, K.; Wada, N.; Tokumoto, H.; Takai, T.; Mizoguchi, T.; Tamiaki, H. Photocatalytic Degradation of Methylene Blue by TiO_2 Film and Au Particles-TiO_2 Composite Film. *Thin Solid Films.* **2008**, *516*, 5881–5884.
(41) Marbán, G.; Vu, T. T.; Valdés-Solís, T. A Simple Visible Spectrum Deconvolution Technique to Prevent the Artefact Induced by the Hypsochromic Shift from Masking the Concentration of Methylene Blue in Photodegradation Experiments. *Appl. Catal. A Gen.* **2011**, *402*, 218–223.
(42) Patil, K.; Pawar, R.; Talap, P. Self-Aggregation of Methylene Blue in Aqueous Medium and Aqueous Solutions of Bu_4NBr and Urea. *Phys. Chem. Chem. Phys.* **2000**, *2*, 4313–4317.
(43) Junqueira, H. C.; Severino, D.; Dias, L. G.; Gugliotti, M. S.; Baptista, M. S. Modulation of Methylene Blue Photochemical Properties Based on Adsorption at Aqueous Micelle Interfaces. *Phys. Chem. Chem. Phys.* **2002**, *4*, 2320–2328.
(44) Severino, D.; Junqueira, H. C.; Gugliotti, M.; Gabrielli, D. S.; Baptista, M. S. Influence of Negatively Charged Interfaces on the Ground and Excited State Properties of Methylene Blue. *Photochem. Photobiol.* **2003**, *77*, 459–468.

(45) Greci, L. On the Use of 1, 3-Diphenylisobenzofuran Reactions With Carbon and Oxygen Centered Radicals in Model and Natural Systems. **1993**, *19*, 395–405.
(46) Nuñez, S. C.; Yoshimura, T. M.; Ribeiro, M. S.; Junqueira, H. C.; Maciel, C.; Coutinho-Neto, M. D.; Baptista, M. S. Urea Enhances the Photodynamic Efficiency of Methylene Blue. *J. Photochem. Photobiol. B Biol.* **2015**, *150*, 31–37.
(47) Mundra, V.; Li, W.; Mahato, R. I. Nanoparticle-Mediated Drug Delivery for Treating Melanoma. *Nanomedicine.* **2015**, *10*, 2613–2633.
(48) Kang, W.; Svirskis, D.; Sarojini, V.; McGregor, A. L.; Bevitt, J.; Wu, Z. Cyclic-RGDyC Functionalized Liposomes for Dual-Targeting of Tumor Vasculature and Cancer Cells in Glioblastoma: An in Vitro Boron Neutron Capture Therapy Study. *Oncotarget.* **2017**, *8*, 36614–36627.
(49) Chen, F.; Ma, K.; Benezra, M.; Zhang, L.; Cheal, S. M.; Phillips, E.; Yoo, B.; Pauliah, M.; Overholtzer, M.; Zanzonico, P.; Sequeira, S.; Gonen, M.; Quinn, T.; Wiesner, U.; Bradbury, M. S. Cancer-Targeting Ultrasmall Silica Nanoparticles for Clinical Translation: Physicochemical Structure and Biological Property Correlations. *Chem. Mater.* **2017**, *29*, 8766–8779.
(50) Ow, H., Larson, D. R., Srivastava, M., Baird, B. A., Webb, W. W., & Wiesner, U. (2005). Bright and Stable Core−Shell Fluorescent Silica Nanoparticles. *Nano Lett.* **2005**, *5*, 113–117.
(51) Larson, D. R., Ow, H., Vishwasrao, H. D., Heikal, A. A., Wiesner, U., & Webb, W. W. (2008). Silica Nanoparticle Architecture Determines Radiative Properties of Encapsulated Fluorophores. *Chem. Mater*. **2008**, *20*, 2677–2684.